JET–P(98)86

G Saibene et al

The Influence of Isotopic Mass, Edge Magnetic Shear and Input Power on High Density ELMy H-modes in JET

JET–P(98)86

The Influence of Isotopic Mass, Edge Magnetic Shear and Input Power on High Density ELMy H-modes in JET

G Saibene, L D Horton, R Sartori, B Balet, S Clement, G D Conway, J G Cordey, H P L de Esch, C Ingesson, J Lingertat, R D Monk, V Parail, R Smith, A Taroni, K Thomsen, M von Hellermann.

JET Joint Undertaking, Abingdon, Oxfordshire, OX14 3EA,

Preprint of a Paper submitted for publication in Nuclear Fusion

February 1999

ABSTRACT

This paper presents the results of experiments carried out in JET with the Mark II divertor to study ELMy H modes at high density. In these experiments we varied the effective ion mass of the plasma (pure H, D and T), the input power, plasma current and the edge magnetic shear. The variation of density was achieved by gas fuelling.

The paper focuses on two main issues: the variation of the global energy confinement with density and the scaling of the H mode pedestal. We find that the density dependence in the ITER97-p(y) scaling is not confirmed by the experiment when one approaches the density limit. For the high density regime in ELMy H-modes we propose a density independent scaling that includes the plasma triangularity in the regression variables. The core energy content of the plasma is correlated to the edge pedestal parameters, consistently with a mixed Bohm-gyroBohm transport model for H mode plasmas.

It is found that with type I ELMs, the edge pedestal pressure increases with the ion mass of the plasma, the input power and the edge magnetic shear. We have derived a scaling for the edge pedestal width starting from the measured pressure at the top of the pedestal and assuming that the critical pressure gradient in the pedestal is determined by ideal ballooning modes. We find that the measured decrease of the edge pedestal pressure with density during Type I ELMs can be described by a model where the reduction of the edge pedestal width is due to the decrease of the ion temperature at the edge. In particular, the best fit to the data is obtained assuming that the pedestal width scales with the poloidal Larmor radius of the ions.

1. INTRODUCTION

ELMy H-modes at high density are one of the possible scenarios for the operation of a future fusion reactor [1] since they have the potential to combine quasi-steady state plasma conditions with high fusion reactivity. In present-day tokamaks and in JET in particular, dedicated experiments have been carried out to the study of the characteristics of ELMy H-modes, including plasmas at the highest attainable densities [2-8].

In JET, the plasma density of an ELMy H-mode with neutral beam heating and without additional fuelling is observed to maintain a ‘’natural’’ value [9], determined by confinement and wall recycling, generally of about 50% of the Greenwald density limit [10] ($GDL = I_p/(\pi a^2)$, 10^{20} m^{-3} MA, m, a= plasma minor radius and I_p = plasma current).

In the Type I ELM regime (refer to [11] and [12] for reviews on ELMs and their classification), the global energy confinement of the discharge is good (H97 ~1, [13]) and the density and stored energy are in steady state. Unfortunately, for typical JET ELMy H-modes, the expulsion of energy associated with Type I ELMs is of the order of 3%-10% of the plasma stored energy. The best case scenario for the extrapolation to a reactor translates to only marginally acceptable power loads to the plasma facing components of the divertor [14].

When external gas fuelling is applied to these discharges, the frequency of Type I ELMs increases while the energy confinement of the plasma is somewhat reduced. Further increase of the external fuelling source is associated with a transition from type I to type III ELMs [15], and to a further reduction of the plasma energy content, compared to the Type I ELM phase. Although the small and frequent type III ELMs associated with the high density phase of ELMy H-modes have the advantage of a much reduced peak power load on plasma facing components, the deterioration of the energy confinement makes this regime less favourable for the design of future reactors. In extreme cases, for very high fuelling rates, the confinement for energy and particles is reduced to a point where the average plasma density decreases and a back transition from H to L-mode is observed [16-17].

The maximum density achieved in gas fuelled steady state ELMy H-modes in JET is ~95% of the *GDL*. A characteristic feature of ELMy H-modes at high density is the resilience of the plasma to the externally applied particle source, resulting in an effective saturation of the plasma density n_e. The process leading to this saturation is not well understood, although results from trace tritium injection experiments in high density ELMy H-modes indicate that the failure to increase the density is not due to a fuelling limit [18]. Plasma densities above the *GDL* were achieved in ASDEX-Upgrade [17] by means of deuterium pellet injection in ELMy H-modes, but with a similar degradation of the energy confinement time as for the gas fuelled cases.

Experiments on high density ELMy H-modes have been carried out in JET since the installation of the internal pumped divertor. The effects of the divertor geometry have been investigated by installing a succession of more closed divertors (called Mark I, Mark II and the latest Mark IIGB [8]). In this paper we present the results of experiments aimed at the study of the global and local confinement of ELMy H-modes as a function of density, power, hydrogen isotope and plasma shape, carried out in the JET Mark II campaign (MkII).

The details of the experiments are described in section 2.1. In particular, we focus on three series of experiments. In the first, the main plasma parameters were maintained constant and the composition of the plasma was in turn pure H, D and T. The other two series of experiments, in D, were dedicated to the study of the effects of the plasma triangularity and power on density and confinement. The general results of the experiments are described in section 3, and compared to the large JET database of gas fuelled ELMy H-modes in deuterium. The experimental results are compared with global confinement scaling laws in section 4. The variation of the effective mass number of the plasma ions, shape and input power are explored in section 5, where models for the scaling of the edge pedestal at the ballooning limit are compared to the experimental data. Lastly, results from EDGE2D [19] simulations of H-modes with the three isotopes are presented and discussed (section 5.4).

2. EXPERIMENT

2.1. General description of the experimental parameters

Three series of experiments are presented in detail: an isotope mass scan, a triangularity scan and a power scan.

In these experiments, we carried out pulse-to-pulse gas fuelling scans, keeping the gas fuelling constant in each discharge. For all the experiments, the in-vessel divertor cryopump was used, either at its full pumping capacity or half of it. As it will be shown in section 2.2, the variation in pumping speed affects the level of recycling from the walls, but does not otherwise influence the results presented.

The first series of experiments, investigated during the Deuterium Tritium Experiment 1 (DTE1) campaign in JET [20], was the study of the mass dependence of main plasma parameters of ELMy H-modes with increasing external fuelling. To maximise the mass effects and obtain pure plasmas of each isotope, preparatory discharges were carried out to change the wall recycling to ~100% pure H, D and T in turn (see section 2.2). The data in this series originate from two sets of discharges. In the first set, the plasma current was I_p=2.6MA, the toroidal field B_t=2.7T, (q_{95}=3.4, where the suffix indicates that the safety factor is calculated at the magnetic surface corresponding to 95% of the flux), and neutral beam heating power P_{in} ~12MW, for deuterium and tritium plasmas. In the case of hydrogen plasmas, technical constraints of the neutral beam heating systems limited the amount of injected power to ~10-11MW. In order to obtain Type I ELMy discharges in hydrogen (see section 2.1.1), the second set of plasma discharges was carried out at reduced plasma current and toroidal field (I_p=1.7-1.8MA, B_t=1.7-1.8T, i.e. at the same q_{95} as in the first set) and at similar neutral beam power levels. In each case, reference H-modes were obtained without external gas fuelling, and then the gas flow rate was increased from pulse to pulse, to the level required to obtain Type III ELMs or the H→L back transition. The maximum amount of external gas fuelling used in the gas scans is limited by technical constraints. In particular, the gas injection causes an increase in the neutral pressure in the NB system injection ducts, so that local power deposition due to beam ionisation exceeds the maximum permissible amount.

The divertor plasma geometry selected for the experiment was a single null, with the separatrix on the horizontal target plates and x-point to tile distance of about 8cm (in the poloidal plane). The average plasma triangularity was fixed at δ=0.32 ($\delta = 0.5(\delta_{upper} + \delta_{lower})$), calculated at the separatrix.

The effects of triangularity are studied in the second series of experiments presented. Gas scans were performed at 2.6MA/2.7T and constant neutral beam input power of ~12MW, where the average triangularity was varied from ~0.14 to 0.38, corresponding to an increase of the edge magnetic shear Sh_{95} from ~2.9 to 4.1 (Sh_{95} is the average shear calculated over a magnetic surface corresponding to 95% of the flux).

Finally, the third series of experiments studied the effects of gas fuelling at three different levels of input power, 8, 12 and 14MW. The discharges were carried out in pure D at 2.6MA/ 2.7T, at constant plasma shape (δ =0.23) and divertor configuration (strike points on the horizontal plates).

The analysis of the energy confinement of high density ELMy H-modes (section 4) is carried on an extended database. This database includes all the NB heated gas scans carried out in JET in the MkII experimental campaign that reached steady state conditions. The dataset includes a total of 145 plasma discharges, with plasma parameters spanning a large range (as detailed in table I), although a large majority of pulses is in pure D, and about 2/3 of the pulses have I_p ~2.5MA. The data from the three main experiments described at the beginning of this paragraph are included in the database.

Table I: Range of parameters in the gas fuelled dataset of ELMy H-modes. The parameters in the table are defined in the text

Variable	Minimum	Maximum
I_p (MA)	1.5	3.7
B_t (T)	1.5	3.6
A_{eff}	1	3
n_e (10^{19}m^{-3})	1.8	9.2
$n_e/n_{e,GR}$ (%)	35	98
P_{Loss} (MW)	7	17
δ	0.13	0.38

2.1.1. The Hydrogen experiment: accessibility of the Type I ELM regime

Experiments with different isotopes carried out at the same input power, density and toroidal field are characterised by a varying amount of power above the H-mode power threshold. This is due to the dependence of the H-mode threshold on the Hydrogenic isotope mass [21], $P_{th} \propto (A_{eff})^{-1}$ (where $P_{th} = (P_\Omega + P_{in} - dW/dt)$, calculated at the L→H transition and A_{eff} is the effective ion mass number of the plasma). In the case of the 2.6MA/2.7T series of pulses, P_{net} in steady state (defined as $P_\Omega + P_{in} - P_{th}$, with P_{th} calculated according to [21]) varied from 6.3-7.3MW for pure T plasmas, to 4.3-5.5MW for D, down to 1.6-3.4MW for H plasmas. In each case, the lower value of P_{net} is calculated at the highest steady state density and the highest corresponds to the lower value of the density, obtained with fuelling provided only by neutral beam injection.

With reference again to [21], it is also found that the power threshold for the transition from type III ELMs (or transition ELMs) to type I ELMs, $P_{th,I}$, increases with mass, similarly to

the L→H transition. Although the data available do not allow the formulation of a precise scaling, it is found that $P_{th,I}$ is ~30% higher than P_{th}.

If one applies these scalings to the two sets of experiments described above, it is found that $P_{in} > P_{th,I}$ for D and T plasmas both at 2.7 and 1.8T, while in the case of H plasmas at 2.7T the amount of power available is sufficient to obtain the L→H transition, but not type I ELMs. In contrast, in H at 1.8T and P_{in} ~10MW, P_{net}~3.5-4.5MW, that is of the order of the net power required for the transition to type I ELMs.

2.2. Particle Balance and Control of the Isotopic Composition of the Plasma

The control of the plasma isotopic content was achieved by changing the composition of the recycling flux from the plasma-facing surfaces to be the same as the desired isotopic composition of the plasma. In the specific case of the D→T wall change over, this was achieved in approximately 30 discharges fuelled with pure T_2 gas, injecting ~1.5 10^{23} T atoms in the SOL, leading to a plasma composition T/(H+D+T) ≥ 95%. During the actual experiment, the plasma was fuelled with pure T_2 gas. The neutral beam injection was predominantly of T_o, with a small fraction (<30%) of the power being injected by D_o beams in some cases, to top up to the required power. For all the T pulses analysed, A_{eff} is ~2.9. Similar plasma purity was obtained for hydrogen and deuterium plasmas, with A_{eff} ~1.05 and ~2.0 respectively.

The magnitude of the total recycling flux in the divertor is comparable to the externally applied gas fuelling rate in steady state. For example, in the case of D, 1.8MA/1.8T plasmas, with the two divertor cryopumps at LHe temperature, the total ion flux to the divertor, measured by Langmuir probes, is of the order of 4 $10^{22}s^{-1}$ without gas fuelling, to be compared to gas injection rates $0 \leq \Phi_{gas} \leq 3.5\ 10^{22}s^{-1}$. For comparison, the neutral flux to the plasma with neutral beam injection is typically ~$10^{21}s^{-1}$.

The contribution of the recycling flux to the particle balance of the plasma can be estimated by comparing the change in the plasma particle content during the initial ELM free phase of the H-mode to the beam fuelling rate, in the absence of additional gas fuelling. For the conditions described above, we find that the plasma inventory increases at a rate that is of up to twice the beam fuelling, demonstrating that the control of the isotopic composition of the wall recycling is essential to control the plasma isotopic ratio.

The ‘’base level’’ of recycling is determined by the balance between the external fuelling, the wall retention and active pumping during plasma and between discharges. During the DTE1 campaign, JET was operated for long periods with only one cryopump cooled to LHe temperature, to reduce the T_2 gas consumption and for compatibility with previous experiments. For comparison purposes, gas scans in D were also carried out with only one divertor cryopump active. The reduction in pumping corresponds to an increase of the neutral flux from the walls (both main chamber and divertor) as shown in figure 1 for the case of divertor fluxes. The largest difference is observed in the absence of external gas fuelling, while the enhancement of recycling due to external sources dominates for large gas rates.

The increase in the base level of recycling changes the ‘’natural density’’ of the plasma (steady state density without gas fuelling) and reduces the window of obtainable densities. As can be seen in figure 2, the minimum density obtained without gas fuelling increases from ~45% to 55% of the *GDL* (from ~4.5 $10^{19}m^{-3}$ to ~5.3 $10^{19}m^{-3}$). The relationship between confinement and density is independent of the gas fuelling.

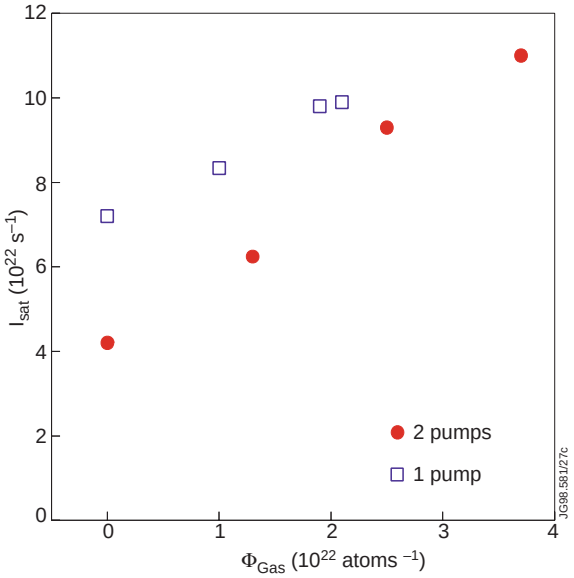

Figure 1: Total ion flux to the divertor as a function of the external fuelling rate, for two series of gas fuelled ELMy H modes in D, 1.8MA/1.8T and ~11MW NBI, with 1 and 2 divertor cryopumps. The data are taken as average during the steady state phase of each discharge. Some points are averages of more than one discharge.

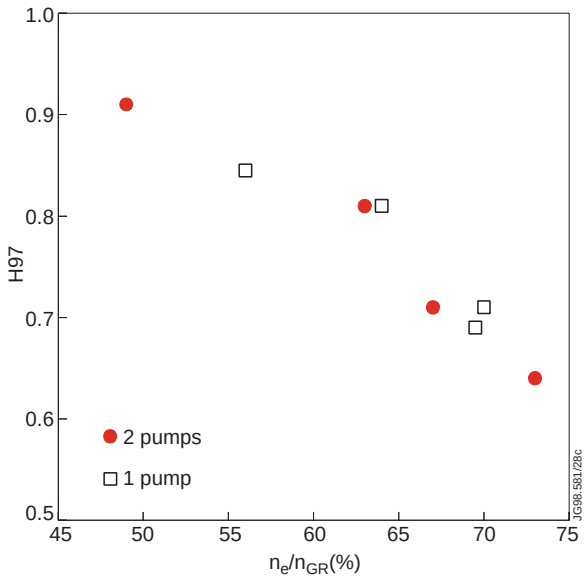

Figure 2: Variation of the confinement enhancement factor H97 as a function of the fraction of the Greenwald limit for the two sets of plasma discharges with 1 and 2 divertor cryo-pumps on.

2.3. Diagnostics and data analysis tools

Most of the standard diagnostics of JET are tritium compatible and were available for the DTE1 experiments. Of particular interest for the analysis of ELMy H-modes are: electron density, electron and ion temperature (bulk and edge), H_α-D_α-T_α emission in the plasma edge, divertor target Langmuir probe data and plasma stored energy.

Density measurements are provided with a FIR interferometer [22] (with 0.5-1.5ms time resolution, depending on the discharge), along several lines of sight. The measurements of the outermost vertical channel (average over ~5cm at R ~3.75m) are used to estimate the pedestal line averaged density. The edge electron temperature profile is measured with high time and spatial resolution (1cm and 10μs respectively) by a heterodyne radiometer [23]. The edge T_e profiles are also used to identify the spatial location of the top of the pedestal, as shown in figure 3, by linear interpolation of the data points.

Unfortunately, at low toroidal field (< 2.0T) the typical edge density achieved in these experiments is higher than the cut-off density for the ECE emission from the edge. In this case,

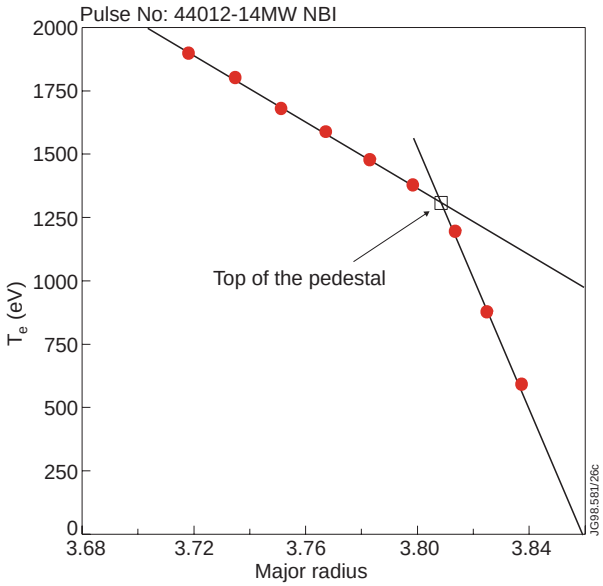

Figure 3: Electron temperature profile measured with the ECE heterodyne radiometer. This profile is taken during the steady state phase of an ELMy H mode (#44012,14MW NBI), in between two Type I ELMs. The open square indicates the extrapolated position of the top of the edge pedestal.

the edge n_e and T_e are taken from LIDAR profile measurements [24], at the fixed location R=3.75m (i.e. at the same tangency point of the FIR outer channel). The accuracy in the determination of the pedestal electron density and temperature is reduced, due to the low repetition rate of the measurement (250ms).

The edge T_i profiles are measured by active charge-exchange spectroscopy [25]. Analysis of typical high density ELMy H-modes [16] has shown that at the pedestal, $T_i \sim T_e$, within the accuracy limits due to the reduced time resolution of the T_i measurement (~400ms). The approximation $T_i \sim T_e \sim T_{ped}$ at the top of the pedestal has been used in the analysis.

In the data analysis presented in sections 3 and 5 we use the following definitions:

- $\langle p_{ped} \rangle \equiv$ the time average over several ELMs of the total thermal plasma pressure calculated at the top of the pedestal; the time window is usually ~1s, during the steady state phase of a discharge.
- $p_{ped,MAX} \equiv$ the value of the pedestal pressure just before an ELM. When the contribution of the fast ions is included in the calculations, this is stated explicitly.

The global confinement analysis is carried out using the latest ITER confinement scaling law (ITER97-P(y)) in [13]. The correction to the plasma stored energy for fast ions is derived from the calculated fast ion distribution in the plasma (in space and velocity), from the Fokker-Plank routines in the PENCIL code [26]. For the type of plasmas in this analysis, the fast ion contribution to the stored energy is relatively low, varying typically from ~15% down to <5% at high density [7]. PENCIL results are also used to estimate the average energy and density (T_{fast} and n_{fast}) of the fast ions in the edge pedestal region. Further analysis of the data was carried out with the transport code TRANSP [27], in particular to check for data consistency.

3. GENERAL RESULTS

The Greenwald density limit has not been exceeded in JET, in steady state ELMy H-modes, with edge gas fuelling, but only transiently at low plasma current [28]. The increase of the density in this plasma regime has some typical effects, which are independent of the specific details of the experiment (power, plasma shape, isotope and divertor configuration).

In section 3.1 we describe the effects of the increased density on the bulk and edge parameters, in particular focusing on the change in the ELM frequency and type.

In section 3.2 the energy confinement of the discharges is analysed in terms of the ITER97-P(y) scaling for the three hydrogen isotopes. Finally, the effects of the plasma triangularity on plasma density, stored energy and ELMs are described in section 3.3.

3.1. Effect of density

3.1.1. Type I and type III ELM regimes

In the absence or at low levels of external gas fuelling the discharge in steady state is characterised by Type I ELMs. As the density is raised (but still substantially below the *GDL*), we observe a decrease of the central T_i and T_e, accompanied by a strong reduction of the sawteeth period and magnitude, and by some decrease of the plasma thermal stored energy (this is discussed later in the paper).

At the plasma edge pedestal, the density increase is accompanied by a cooling of both ion and electrons, and in general by some decrease of the total pedestal pressure p_{ped} (both peak and average values). As the pedestal becomes denser and cooler, the Type I ELM frequency increases, as shown in figure 4.

When the density is increased further, a transition from Type I to Type III ELMs occurs (identified by the arrows in figure 4). We identify these ELMs as Type III, since their frequency decreases with input power, following the standard classification of ELM types [11]. The transition is usually accompanied by an increase in the total radiated power, although the fraction of power radiated by the plasma tends to remain low, typically <50% of P_{in}. Tomographic recon-

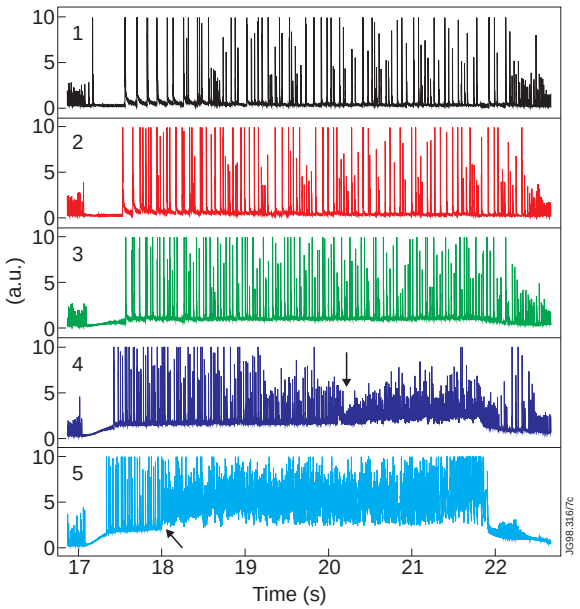

Figure 4: Divertor Balmer-α emission for a series of ELMy H modes. I_p=2.6MA, B_t=2.7T, P_{in}=11MW, δ~ 0.23, with increasing gas fuelling. Note the transition to high density Type III ELMS in the last two pulses of the series shown by the arrows.

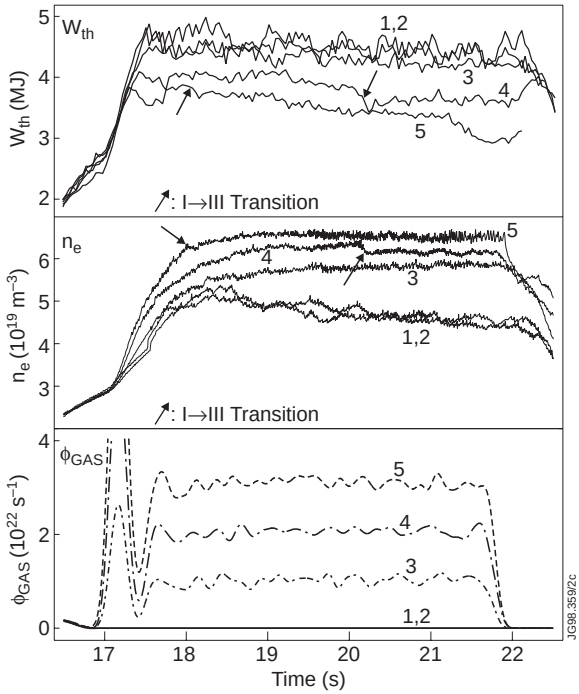

Figure 5: Thermal stored energy (W_{th} (MW)), central line average density (n_e ($10^{19}m^{-3}$)) and gas flow rate for the same discharges as in figure 4

struction of the radiation shows that the increase in the total radiated power is mainly due to increased radiation in the divertor region, both from the x-point and the outer divertor leg. MARFEs are not observed during the H-mode phase of the discharge. Both Type I and Type III ELMy regimes can be sustained in steady state, as shown in figures 4 and 5.

The transition to Type III ELMs is characterised by enhanced edge cooling (compared to the Type I ELMy phase) which is not compensated by the increasing density, and therefore by further loss of pedestal pressure compared to the reference value obtained during unfuelled discharges. The physical mechanism underlying the change in the ELM character is not fully understood at present.

Experimental observations in JET show that the transition from Type I to Type III ELMs is accompanied by an increase of the edge collisionality ν. A model that correlates high density Type III ELMs to the onset of resistive ballooning instabilities at the plasma edge has been proposed in [15]. This model, based on similarity of edge transport mechanisms, provides a scaling of the critical density for the Type I to Type III transition, where it is assumed that Type I ELMs are correlated to ideal ballooning instability and Type III ELMs to resistive ballooning instabilities. The similarity parameter describing the onset of resistive mode is assumed to be the edge collisionality, and the transition to occur when the edge collisionality exceeds a certain critical value. The scaling expression in [15] for the transition from Type I to Type III ELMs reproduces the JET data satisfactorily.

The detailed MHD analysis carried out on type III ELMs [29] and Type I ELMs [30] in ASDEX-U shows that Type III ELMs are triggered at a critical edge pressure gradient much lower than for Type I ELMs. This finding is in qualitative agreement with the hypothesis that Type I ELMs occur near the ideal ballooning limit, while Type III may be by resistive instabilities, therefore occurring at lower edge pressure gradients [31], [12].

Increasing the external fuelling even further may bring the pedestal temperature T_{ped} down near the critical temperature for the H→L transition. When this occurs, we observe first a clamping of T_{ped} and a reduction of the edge density n_{ped} (i.e. a reduction in p_{ped}) and eventually the H→L mode transition. The occurrence of the H→L transition is inconsistent with the expectations from the H-mode threshold power scaling, since the power input in the experiments described is always above the calculated power required to maintain an H-mode (see section 2.1.1). This result is similar to those reported by ASDEX-U [17] for high density ELMy H-modes, and suggests that more work is needed to extend the predictions of the H-mode power threshold to plasmas at densities near the *GDL* and to resolve the inconsistency between the global power scaling of the H-mode threshold and the local temperature scalings.

3.1.2 A typical case of strong fuelling in D

A good illustration of the changes in both the bulk and the edge of an ELMy H-mode plasma with strong fuelling is provided by pulse #44371. This is a 2.6MA/2.7T, 12MW P_{in}, strongly

shaped (δ=0.38) plasma. A very high gas fuelling rate (Φ_{gas}~4 $10^{22}s^{-1}$) was applied from 20s in the discharge.

As shown in figure 6, this particular discharge does not reach steady state, but transiently goes through all the typical phases of a high density ELMy H-mode, as described above. In particular, the plasma line average density keeps increasing after the transition from type I to Type III ELMs (~20.8s), while the stored energy is constantly declining. A strong deterioration of the particle confinement, corresponding to a net decrease of the plasma particle content (after ~22s, figure 6), occurs only near the H→L transition, identified by the step down of the pedestal temperature at ~22.95s (figure 7). The global behaviour of the energy confinement and of the bulk density is reflected in the time evolution of the plasma parameters at the edge pedestal.

This is shown in figure 7, where T_e, n_e, p_{ped} and ν at the position of the edge pedestal are shown. The normalised collisionality ν is defined as $\nu=C_1\backslash Rn_e/(36e^2\pi T_e^2)$ and $C_1=3\sqrt{2}\pi^{5/2}e^4Z_{eff}\ln\Lambda_{e,i}/\varepsilon_o^2$.

In contrast to the bulk parameters, it appears that the plasma pedestal pressure reaches a steady state during the Type I ELMy phase. Approximately 100ms before the onset of Type III ELMs, n_e starts to increase while T_e decreases, resulting in an increase of ν at constant p_{ped}.

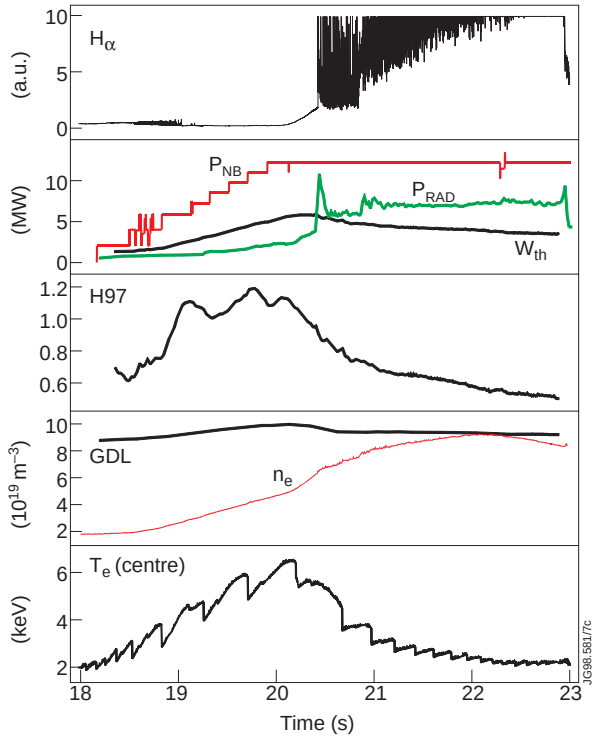

Figure 6: Global parameters for JET pulse #44371: Divertor Balmer-α emission (the signal saturates), input power, total radiated power and thermal stored energy (P_{in}, P_{rad} in MW and W_{th} in MJ), confinement enhancement factor H97, calculated Greenwald density limit GDL and line average density (n_e, $10^{19}m^{-3}$), and central T_e (keV). The gas fueling rate, not shown in the figure, is constant from 60s.

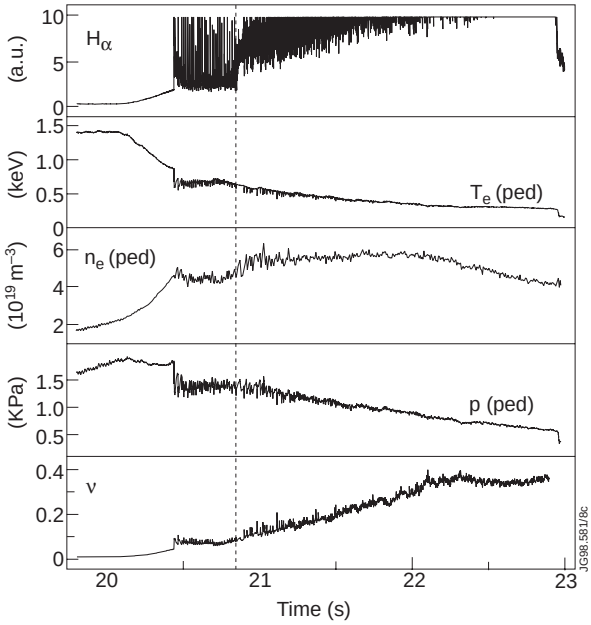

Figure 7: Time traces of edge pedestal parameters for JET pulse #44371. The Balmer-α trace is repeated in box 1 for clarity. In the other boxes: temperature ($T_{e,ped}$ (eV)), density ($n_{e,ped}$ ($10^{19}m^{-3}$)), total thermal pressure (p_{ped} (kPa)) and collisionality (ν), calculated at the top of the edge pedestal. The vertical line marks the transition from type I to Type III ELMs.

During the Type III ELMs, at constant gas fuelling, the temperature of the edge decreases until it reaches ~300eV, i.e. near the critical $T_{e,ped}$ for the L→H transition, for this B_t and n_e [32]. The transition back to L-mode occurs, at constant P_{in}, followed by a classic density limit disruption (not shown in the figure). The disruption occurs at a density lower than the maximum density reached in the H-mode phase, indicating that transport determines the maximum density of H-mode plasmas, in contrast to the conventional MARFE driven instability of L-modes. In fact, the L-mode density limit in the MkII divertor is typically 50-60% of the *GDL*, while in the example the H→L transition occurs at ~80% of the *GDL*. Further evidence for the different physical processes governing the H and L mode density limit is given by the observation of the decreased L mode density limit from MkI to MkII divertors [33], in contrast to the H-mode density limit which did not change with the divertor configuration.

3.2 Isotope mass scan experiments

Gas fuelling scans in ELMy H-modes were carried out in the three hydrogen isotopes, to investigate the isotopic dependence of the H-mode density limit. The results of this experiment confirm the global picture that emerges from the database of D discharges. At low density, the energy confinement enhancement is ~1, according to the predictions of the ITER97-P(y) scaling. With gas fuelling (the external fluxes are of the level of the average recycling flux), the density rise tends to saturate as the confinement enhancement factor of the discharge decreases. This is illustrated in figure 8 for a selection of plasma discharges in pure H, D and T.

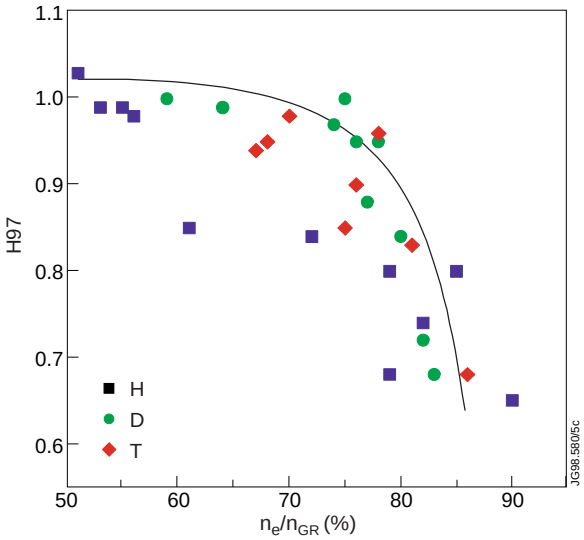

Figure 8: Confinement enhancement factor H97 as a function of the fraction of the Greenwald density limit. Data taken in steady state separated by isotope. The data set in the figure includes discharges with $1.7 \leq I_p$ (MA), B_t (T)≤3. All the discharges included have q_{95} ~3.3 and NB input power of 10-12MW.

Figure 8 includes data from the steady state phase of the gas scan experiments described in section 2.1, and also from other similar ELMy H-modes carried out with the two cryopumps active, to provide comparison data at lower density. For all selected discharges, $P_{in} > P_{th,I}$, and all pulses with external gas fuelling have the same average triangularity.

The degradation of confinement with density occurs in a very similar way for the three isotopes, in particular for D and T. The H data seem to indicate that a significant loss of confinement occurs at lower fraction of the Greenwald limit compared to D and T. However, at high density (≥80% of the *GDL*, when all the discharges in the graph have Type III ELMs), the H97 is very similar for the three isotopes. This confirms and extends to the isotope mass number, the

general result ([34], [7]) that the reduction of the confinement of high density plasmas (compared to the expected scaling) is a general phenomenon, broadly independent of the specific parameters of the discharge, such as the input power, plasma shape and divertor geometry.

The variation of the average mass of the plasma has a very strong effect on the ELMs. This is shown in figure 9, for three steady state ELMy H-modes, with similar input powers and no gas fuelling, in pure H, D and T. The case of H is discussed in more detail in the following section.

The reduction of the ELM frequency for T plasmas compared to D plasmas is associated with an increase of the plasma stored energy at constant input power (6MJ for the T case, compared to 5.4MJ for D). Similar effects are observed in JET when the plasma triangularity δ is increased, as shown in figure 10. This is discussed in section 3.3.

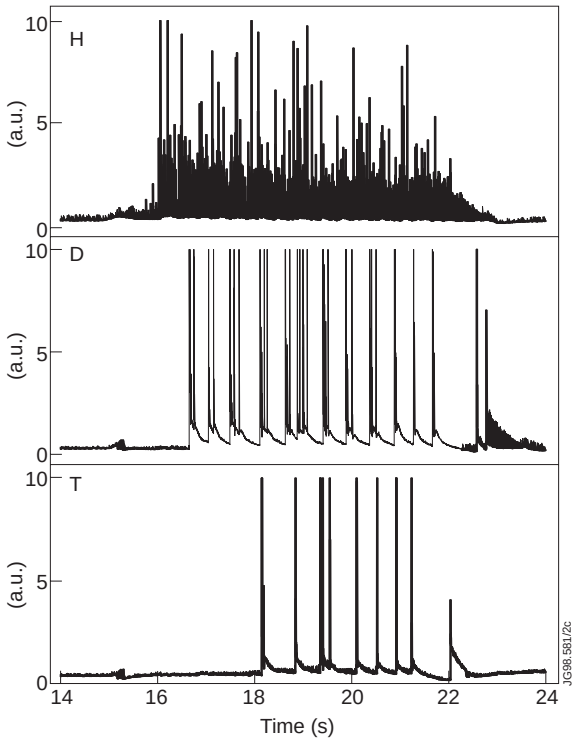

Figure 9: Balmer-α emission for three ELMy H modes (#43392, 43154 and 43003) in pure H, D and T, at 2.6MA/2.7T, no additional gas fuelling. The NB input power is 11-12MW. The different ELM frequency correlates to the change in A_{eff}, although in the case of H, proximity to the H mode threshold also plays a role. The occurrence of composite ELMs for the D and T discharges, is typical of high recycling conditions, when only one cryopump is operational

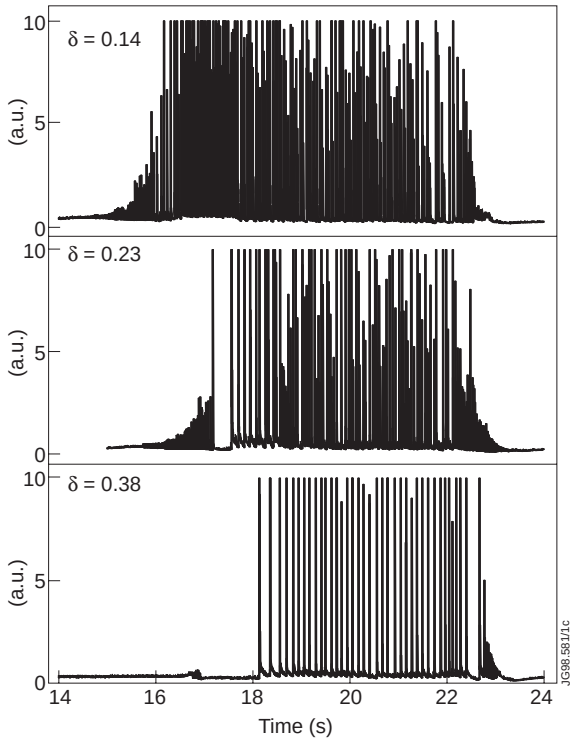

Figure 10: Divertor Balmer-α emission for three ELMy H modes, at 2.6MA/2.7T, Pin ~11-12MW, no additional gas fuelling. The variation in the ELM frequency is linearly correlated to the variation of the plasma δ (#44349-#44028-#44356).

3.2.1 Hydrogen results at 2.6MA/2.7T

The experiments carried out in H at low power above the H-mode threshold (2.6MA/2.7T, 11MW P_{in}) show some differences compared to the discharges in which the power is well above the H-mode power threshold. The H discharges at 2.7T and 11MW of input power go into H-mode and remain in the Type III ELMy regime. Even with no gas fuelling, the global energy confinement

of these discharges is somewhat lower compared to similar discharges in D and T but more importantly, the degradation of confinement with external fuelling is much more severe than for the standard Type I ELMy H-mode. As the external gas fuelling is increased, we observe a saturation of the density at very low values, <50% of the Greenwald limit, and early transition back to L-mode. These results are not yet fully understood, but they highlight the potential difficulty of operation at high density near the H-mode power threshold. More details on the edge parameters of these discharges are contained in section 5.

3.3 Effects of triangularity

The variation of the plasma triangularity in ELMy H-modes is correlated to strong changes in the ELM frequency (see figure 10), density and global energy confinement. To investigate this phenomenon in detail, gas scans were carried out at constant NB input power of 12MW, in four series of discharges in which the triangularity varied from $\delta \sim 0.14$ to $\delta \sim 0.38$ (δ=0.14-0.23-0.32 and 0.38, corresponding to Sh_{95} values of 2.9-3.2-3.8 and 4.1 respectively). The experiment was aimed at achieving steady state conditions, so each value of triangularity was investigated in separate gas scans.

The plasma energy content increases with the edge shear of the discharge. The two extreeme cases in Type I ELMs, the unfuelled and the heavy fuelled plasma, (points labelled ‘’before I to III transition’’) are shown in figure 11.

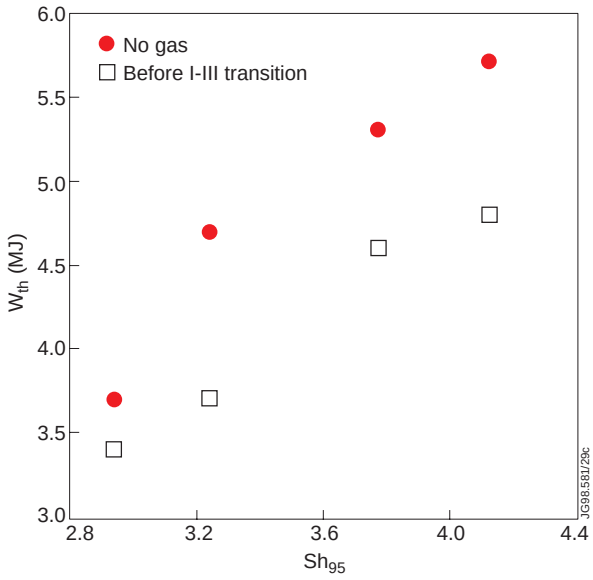

Figure 11: Plasma thermal stored energy W_{th} (MJ) as a function of the edge magnetic shear Sh_{95}, for the no gas discharges, and before the transition from Type I to Type III ELMs, with strong gas fuelling.

At constant power and gas fuelling, the ELM frequency decreases with δ. In the case of unfuelled discharges, the ELM frequency decreases linearly from 25Hz (δ=0.14) to 9Hz (δ=0.38). As expected, less frequent ELMs are associated with larger stored energy loss per ELM. Figure 12 shows that, with no gas, the percentage plasma energy loss is very high at high shear, reaching about 9% for Sh_{95}=3.8. However, strong gas fuelling reduces the differences between high and low shear plasmas, and near the Type I to Type III ELM transition, where $\Delta W/W$ is <3% for all configurations. Shallow pellet injection has also been shown to be effective in increasing the ELM frequency and reducing the peak power deposition per ELM [35], with modest degradation of confinement.

Another effect of increasing the triangularity in ELMy H-modes is that higher densities are reached for the same energy confinement enhancement factor, as shown in figure 13 (from [16]).

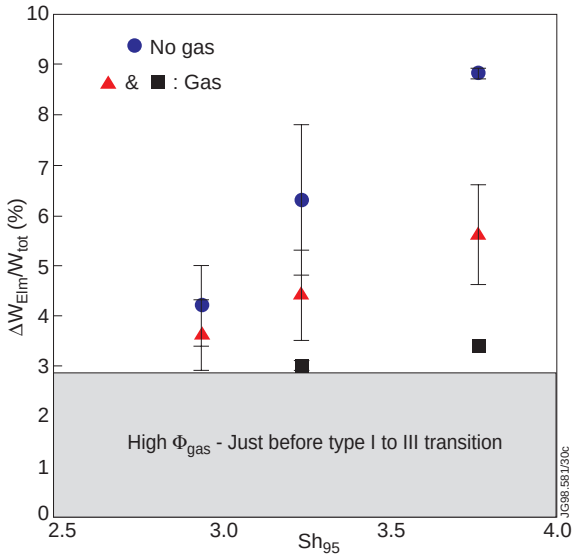

Figure 12: Percentual plasma energy loss per ELM vs. Sh_{95}, Φ_{gas}=0 (circles), Φ_{gas} ~1.2 $10^{22}s^{-1}$ (triangles), and Φ_{gas} ~2.3 $10^{22}s^{-1}$ (squares), in Type I ELM regime. Losses below ~3% of W cannot be measured.

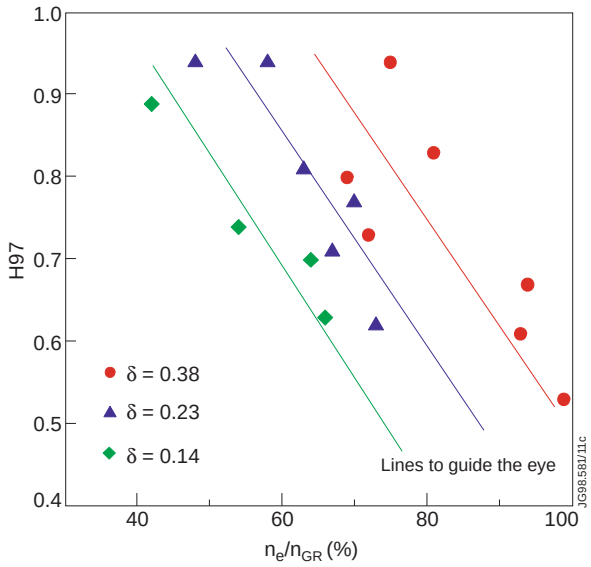

Figure 13: Degradation of confinement as function of the plasma density for three series of gas scans, at 2.6MA/2.7T, P_{in}~12MW, edge δ from 0.14 to 0.38.

The highest H97 for each δ in figure 13 is obtained in the discharges without additional fuelling. Nonetheless the density achieved by the plasma with δ=0.14 is only ~40% of the *GDL*, whilst the density reached about 75% of the *GDL* for δ=0.38. The H97 value for the three discharges without gas is the same. Upon the application of gas, the confinement enhancement factor decreases in all cases with increasing density.

Three main results are obtained from the triangularity scans:

1. The ITER97-p(y) scaling does not allow to discriminate between the increase in density that occurs as a consequence of improved confinement and the increase of density by fuelling. The $n^{0.4}$ dependence for the predicted stored energy in the H97 calculation describes well the unfuelled discharges, because the increase in the triangularity is associated to an increase in the confinement (τ_E goes from ~350ms to ~530ms), corresponding to an increase of both the thermal stored energy and the plasma density. In contrast, the ITER97-p(y) scaling overpredicts the fuelled cases, showing that the improved energy confinement leads to high density, but that the contrary is not true.
2. We observe a decrease of the thermal stored energy with gas fuelling. This is in contrast with the results reported from JT60-U [36], where the deterioration of confinement with density in ELMy H-modes is attributed to the reduction of the fast ion energy content, at constant thermal energy.

3. At constant triangularity, the decrease of H97 with density is too strong if compared with the actual loss of plasma thermal energy. This is a further indication that the positive density dependence of the predicted stored energy in the ITER97-p(y) does not describe adequately the variation of confinement at high density.

Interestingly, JT60-U also reported an increase of the global energy confinement for high triangularity plasmas [2], although in their case the improved confinement is attributed to the formation of an internal transport barrier, not observed in JET.

4. GLOBAL CONFINEMENT

4.1 Discussion of the results of the ITER97-p(y) scaling

We have seen in the previous sections that the ITER97-p(y) scaling does not describe correctly the variations in the thermal stored energy content of ELMy H-modes. In particular, at high densities, the ITER97-p(y) scaling predicts higher stored energies than observed experimentally.

Two further observations can be made. Firstly, the degradation of the energy confinement with density (see figure 8) cannot be ascribed to variations in the power deposition profile. An example of the calculated power deposition profiles for a gas scan in pure T is given in figure 14. The deposition profiles are time-averaged over 1s during the steady state phase of the discharges. Some of the relevant parameters of these discharges are given in table II. The difference in beam penetration between T^o and D^o beams is not significant due to the very similar energy per mass unit in the two cases (46 keV/amu for T and 40 keV/amu for D). The power density profile is virtually identical for all the pulses in the gas scan for $\rho>0.2$, while the small differences in the power density at the very centre of the plasma are not correlated with the variation of either confinement or stored energy.

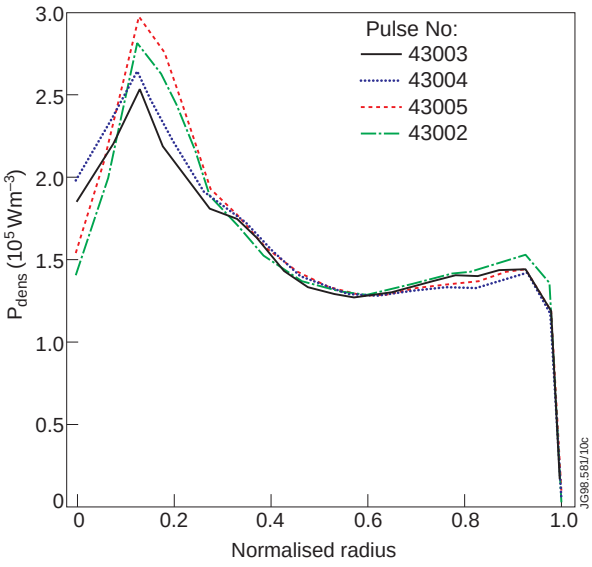

Figure 14: Radial profile of the deposited power density by Neutral Beam injection calculated by PENCIL, for the gas scan series of table 2. The profiles are averaged over ~1s .

Secondly, the variation of the plasma stored energy with triangularity is not predicted by the scaling (see figure 13, where the confinement points for different δ lie on separate curves).

One of the possible reasons for the poor agreement between the measured and predicted confinement enhancement for the high density ELMy H-modes is the composition of the dataset used for the derivation of the ITER97-P(y) scaling. In the particular case of the JET data, the discharges selected for the database are all without additional gas fuelling [37]. In that case, a

strong correlation between global energy and particle confinement is found, which may justify the positive dependence of the predicted plasma stored energy on the average density [38]. This, as we have seen, is not the case for the high density ELMy H-modes.

Table II: Some details of the gas scan in pure tritium.

Pulse #	43003	43004	43005	43002
Φ_{Do} ($10^{22}s^{-1}$)	0	0.7	1	1.4
$n_e/n_{e,GR}$ (%)	76	75	81	86
H97	0.9	0.85	0.83	0.68
P_{in} (T^o, MW)	10.5	10.5	8	8
P_{in} (D^o, MW)	0	0	3	3
ELM Type	I	I	I+III	III

4.2 New scaling

To investigate further the variation of the global confinement of ELMy H-modes, including the discharges with high density, we have analysed the database of all the steady state NB heated gas scans described in section 2.1, that includes both Type I and Type III ELMy discharges.

Firstly, we carried out a log-linear regression on this data using the same variables of the ITER97-P(y) scaling, imposing the ITER97-P(y) values of the exponent for the major radius R, the elongation ε and the aspect ratio κ, since the variation of these parameters in our dataset is too small for carrying out a meaningful fit. The resulting regression is quite different from the ITER97-P(y) scaling, in particular we find no density dependence ($n_e^{0.02\pm0.06}$ in contrast to $n_e^{0.4}$), and both a stronger I_p and A_{eff} dependence than in ITER97-P(y) (from $(A_{eff})^{0.2}$ to $(A_{eff})^{0.51}$ and $(I_p)^{0.90}$ to $(I_p)^{1.28}$). Although the statistical quality of the regression is quite good (*RMSE* of 10%), we have strong cross-correlation between n_e and I_p, and B_t and I_p. Nonetheless, restricting the analysis to fixed I_p=2.5MA confirms the weak n_e dependence of the stored energy.

The same set of data was analysed using a reduced set of variables, including δ, based on the results described in section 3.3. We find that the expression that satisfies the high-β Kadomsev constraint and best fits the results of the ELMy H-mode gas scans is:

$$W_{th,fit}=0.075 I_p^{1.34} R^{0.92} B_t^{-0.12} P_{Loss}^{0.32} A_{eff}^{0.51} \delta^{0.45} \quad (1)$$

with RMSE of 11%. The experimental thermal stored energy is compared to the prediction of H97 and of the fitting with equation (1) in figure 15. The ITER97-P(y) scaling overpredicts the expected stored energy systematically for the pulses in the dataset, while the new fit represents a better average of the experimental W_{th}. The scaling expression in equation (1), derived for the restricted set of JET data summarised in table II, satisfies the stochastic (resistive MHD) transport model constraints, in contrast to the Gyro-Bohm character of the ITER97-P(y) scaling.

More work is needed to clarify this issue, in particular to determine in detail how the changes in the edge of the plasma induced by ELMs affect the transport in the plasma core.

Finally, this density independent scaling should be verified in other tokamaks, to test the triangularity dependence of the scaling, and to account for the effects of machine size in a reliable way.

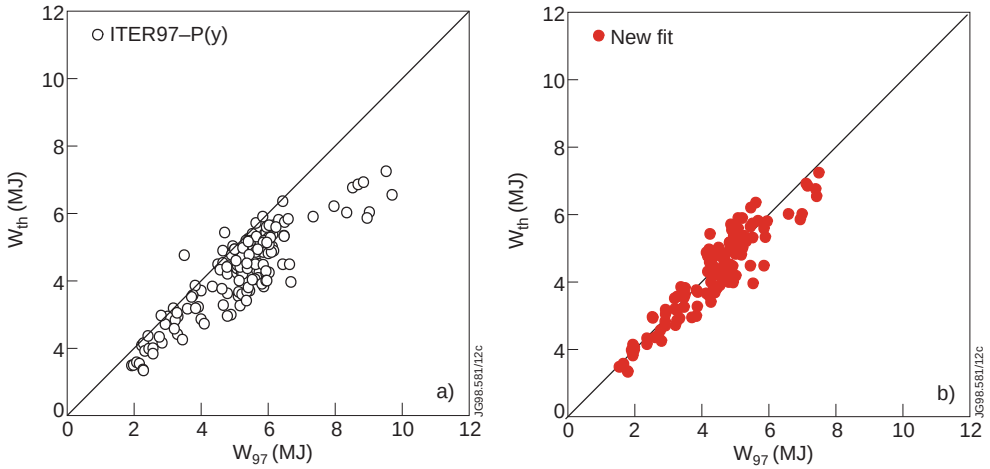

Figure 15: Thermal stored energy vs. predicted stored energy, calculated using the ITER97-P(y) scaling (A) and the scaling proposed in this paper

5. LOCAL EDGE ANALYSIS

5.1 Pedestal energy

We have seen in the previous section that the global confinement in high density H-mode plasmas is best described by a scaling law that, in addition to global parameters, also includes an edge parameter, the edge triangularity. Moreover, the analysis of the variation of the confinement of JET ELMy H-modes at high density or high radiation ([39] and [40]) has highlighted a correlation between the reduction of the confinement and the increase in ELM frequency. In [39], the reduction in the pedestal pressure associated with ELMs is incorporated in an empirical model that describes the decrease of confinement with ELM frequency.

To relate the observed decrease in the global energy confinement to the changes in the edge parameters, we can separate out the pedestal energy content from the total plasma energy content, and analyse how the two components vary with increasing plasma density. A simple way to do this is to assume that the total plasma stored energy $W_{th}=W_{ped}+W_{profile}$, where W_{ped} is the total energy content in the pedestal, defined as $W_{ped}=3/2<p_{ped}>V_p$ where V_p is the plasma volume and $<p_{ped}>$ is the time average plasma pressure, calculated at the top of the edge pedestal. A schematic illustration of the two-term approximation to the total plasma stored energy is shown in figure 16. The components of p_{ped} are the thermal ion and electron pressures ($p_{ped,th}=(p_{i,ped})_{th}+(p_{e,ped})_{th}$). In this paper we use the approximation $n_e \sim n_i$ and $T_i \sim T_e$, $p_{ped,th} \sim 2(p_{e,ped})_{th}$.

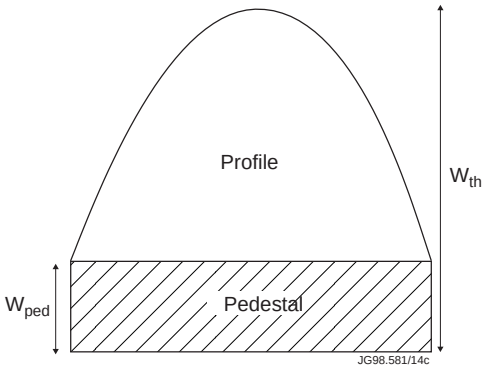

Figure 16: Schematic representation of the pedestal and profile components of the total plasma stored energy. The top of the pedestal, defining the height of the ''plinth" in the figure is identified by the break in the edge electron temperature profile, as measured with the heterodyne radiometer.

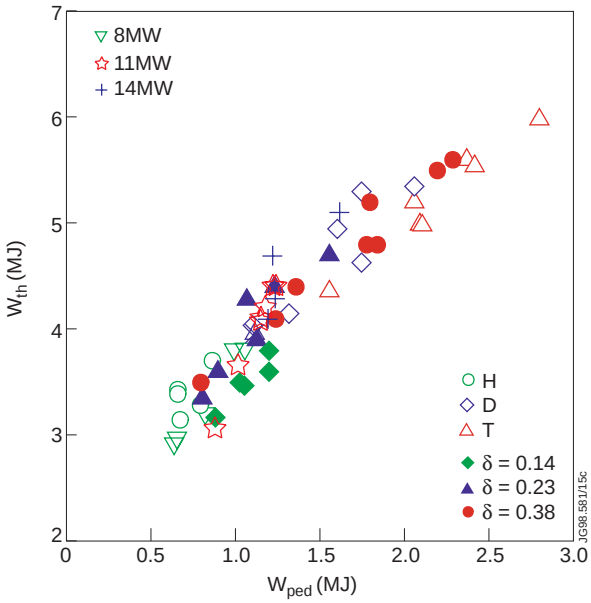

Figure 17: W_{th} as a function of W_{ped} for three series of gas scans in ELMy H modes. The data are averaged over 1s during the steady state phase of each discharge. The decrease of W_{th} and W_{ped} in each series of discharges corresponds to increasing gas fuelling and density.

As expected, we find that the average W_{th} is correlated to W_{ped}, with the higher global stored energy corresponding to higher pedestal energy. This is shown for three sets of experiments in figure 17.

As described in section 2.1, we carried out gas scans in ELMy H-modes at fixed I_p and B_t, varying independently the plasma triangularity δ (at fixed input power, in D), then the input power (at fixed δ, in D), and finally changing the A_{eff} of the plasma from 1 to 3. In each case, we observe a very similar relationship between the pedestal pressure and the global plasma energy content.

For low fuelling rates we find that the decrease in the total plasma stored energy is accounted for by the loss of pedestal energy. In contrast, at the highest densities, in particular after the transition to type III ELMs, the decrease in W_{ped} is not sufficient to explain the global energy confinement losses.

A typical example is given in figure 18 where, for the case of the triangularity scan experiment, we see that the decrease of W_{ped} at high density accounts only for ~70% of the

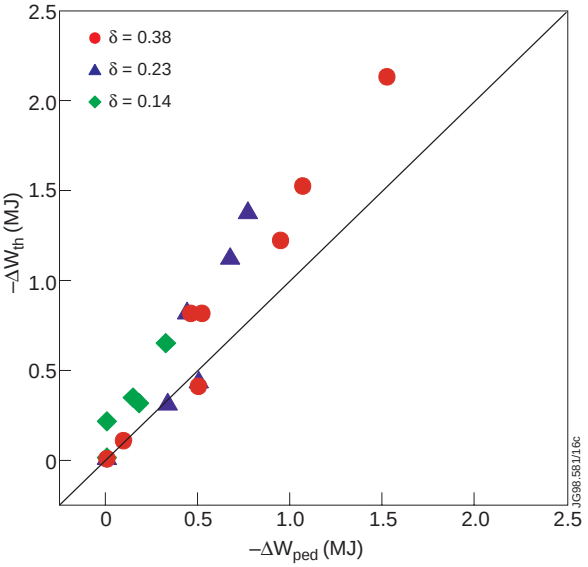

Figure 18: Variation of the total plasma stored energy (ΔW_{th}, MJ) vs. the corresponding variation of the pedestal energy (ΔW_{ped}, MJ), for increasing gas fuelling and density, in the δ scan experiment. The values of W_{th} and W_{ped} for the zero gas case are taken as reference for the calculation.

total plasma energy loss. Plasma density losses greater than the reduction of the pedestal energy occur both during high density Type I ELMs and Type III ELMs. This shows that the degradation of energy confinement at high density is not limited to the pedestal region, but affects the bulk of the plasma. Another experimental indication of the correlation between the pedestal and the profile energy content is provided by the comparison of the W_{ped} and $W_{profile}$ for increasing triangularity. In the particular case of the unfuelled discharges, the increase of the edge triangularity corresponds to an increase of the pedestal energy content as well as of the profile contribution. The increase of W_{ped} is ~50%, going from δ=0.14 to δ =0.38, whilst the corresponding increase of $W_{profile}$ is ~20%.

The changes in the ''profile'' contribution to the total stored energy for increasing density are illustrated in figures 19 and 20, for the case of the pure T ELMy H-mode gas scan. As the density and fuelling increase, an erosion of the plasma pressure profile occurs (figure 19) that is associated with the decrease of the pedestal pressure. This confirms the indications from the analysis of the global and local energy content variation that, at high density, the region of enhanced transport extends somewhat into the plasma core (see also section 5.3). The changes in the profiles would suggest that the region of enhanced transport is limited to R ≥3.5m (or to ρ/a ≥ 0.6).

The degradation of the profile contribution (i.e. inside the edge transport barrier) is limited for Type I ELMy H-modes, and in general the central pressure is not affected, both for electrons and ions. A reduction of the central electron pressure occurs only with Type III ELMs, as shown in figure 20.

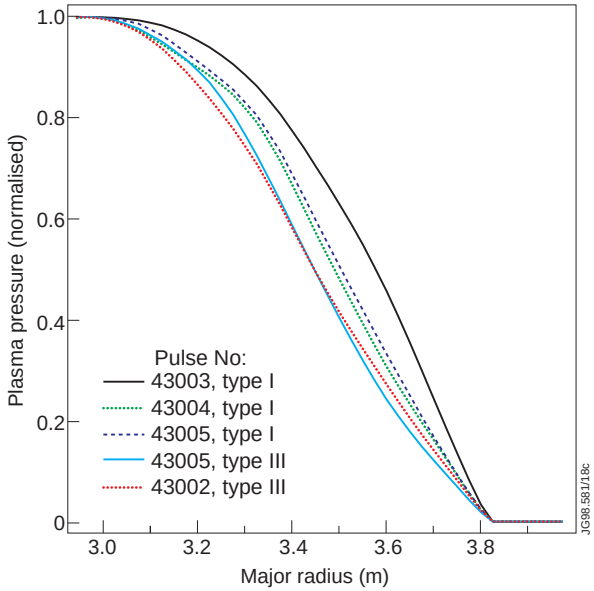

Figure 19: Total plasma pressure profiles for the pulses in table II, calculated by TRANSP. The profiles are smoothed, time averaged and then normalised, to highlight the changes in their shape for increasing density, in particular at the highest density/gas rates with type III ELMs.

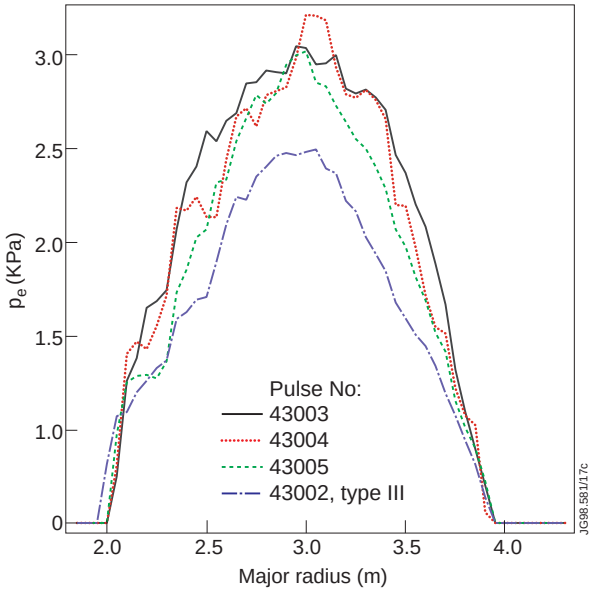

Figure 20: LIDAR electron pressure profiles for the pulses described in table II. The profiles are the time average of several experimental profiles, taken just before an ELM, during the steady state phase of the discharge. For pulse #43002, that has high frequency Type III ELMs, the profiles are taken randomly in the steady state phase of the discharge

5.1.1 W_{ped} in ‘’near threshold’’ conditions

As mentioned in section 3.1, the hydrogen discharges with P_{in} near the H-mode power threshold are characterised by low global confinement and low density. The first observation is that p_{ped} for the pulses at 2.6MA/2.7T is very low, comparable to similar pulses at 1.7MA/1.7T (well above threshold), contrary to the expectations from the scaling that $p_{ped} \propto I_p$ (see section 5.2). Moreover, the maximum edge density achieved in H in these conditions is only about 50% of the density obtained in D and T, and the maximum edge pressure is reduced by approximately a factor of 3 compared to D and T, at the same plasma current and similar total input power. Considering that the global energy confinement of the unfuelled pulses is only ~20% (H97) lower than the D and T cases, it appears that with ‘’near threshold’’ Type III ELMs, the local edge pressure is reduced compared to standard Type I ELM pulses.

In summary, the reduction of the plasma thermal energy content with increasing density is due to a reduction of both the pedestal and the profile energy content. The reduction in the profile energy is more pronounced at very high density, and extends to the centre of the plasma only with Type III ELMs. In the case of H-modes near the threshold, the reduced confinement seems to be mainly due to reduced pedestal energy.

5.2 Edge pedestal scaling

Figure 17 shows that the average plasma pressure at the pedestal can be varied by changing some global plasma parameters, such as the density, input power, the edge magnetic shear or even the effective mass of the plasma, at constant plasma current and magnetic field. This is true also if, instead of considering *average* values of p_{ped}, one analyses the variation of the *maximum* edge pressure (calculated at the pedestal top, just before the ELM) for the same plasma discharges. As already mentioned in section 3.1.1, when the gas fuelling in increased, the pedestal density increases and the pedestal temperature decreases, in such a way that the maximum pedestal pressure decreases. This experimental observation is consistent with the hypothesis that, at least in the case of Type I ELMs, the maximum pedestal pressure is determined by an ideal ballooning limit ([30], [41] and [42]) that is, by a critical edge pressure gradient. Following the simplified approach in [43], one can approximate $(\nabla p)_{crit}$ as $p_{crit}\,\Delta^{-1}$, where Δ is the edge pedestal width, and p_{crit} is identified with $p_{ped,MAX}$, that is with the pedestal pressure just before an ELM (refer to section 2.3). The ballooning stability criterion can then be written as [43]:

$$p_{crit} \propto I_p^{\,2}\, f(sh)\, \Delta \qquad (2)$$

where *f(sh)* is a function of the edge magnetic shear. Using this approach, it is sufficient to assume that the edge pedestal narrows as the edge is cooling ($\Delta \propto (T_{ped})^{x}$), to explain the reduction of $p_{ped,MAX}$ at constant $(\nabla p)_{crit}$, and the corresponding increase of ELM frequency with density. Theoretical models [41] propose that the critical scale-length for the stabilisation of

turbulence in the plasma edge is determined by the poloidal Larmor radius of the locally trapped particles ($\Delta \propto \rho_L \propto I_p^{-1}\sqrt{mT}$, with m=1,2,3), and this approach is adopted in the analysis of the experimental data.

In the following sections we analyse the variation of the maximum pedestal pressure in ELMy H-modes, for the three main experiments described in section 2.1: power, mass and triangularity scans with varying gas fuelling rates. The analysis shows that the variation of $p_{ped,MAX}$ measured experimentally in Type I ELMy discharges is well described by equation 2, if we assume that the pedestal width Δ scales proportional to the ion Larmor radius. In particular, the set of data analysed in this paper favour the hypothesis that thermal ions are responsible for the edge stabilisation mechanism. The hypothesis discussed by [41], [44] and [43], that Δ is proportional to the Larmor radius of the fast ions, does not to describe well our results.

5.2.1 Power scan experiments

The first set of experiments that we analyse is the power scan. For this experiment we observe the familiar reduction of the edge pressure with density, but also that the maximum edge pressure $p_{ped,MAX}$ increases with increasing input power (see figure 17), all other parameters being the same. According to equation 2, we expect that $p_{ped,MAX} \propto \Delta$ since all discharges in this series have the same I_p and shear. Our analysis shows that we obtain a reasonable scaling of $p_{ped,MAx}$ if we assume that Δ scales proportionally with $\sqrt{T_{ped,th}}$, i.e. with the thermal Larmor radius, as shown in figure 21. This result is in good agreement with recent analysis from JT60-U [45]

We find that the variation of $p_{ped,MAX}$ with input power and gas is not well represented by a scaling of the pedestal width with the Larmor radius of the fast ions, in contrast to the findings reported in [43] and [44] (figure 22, where the contribution of the fast ions to the total pressure is included).

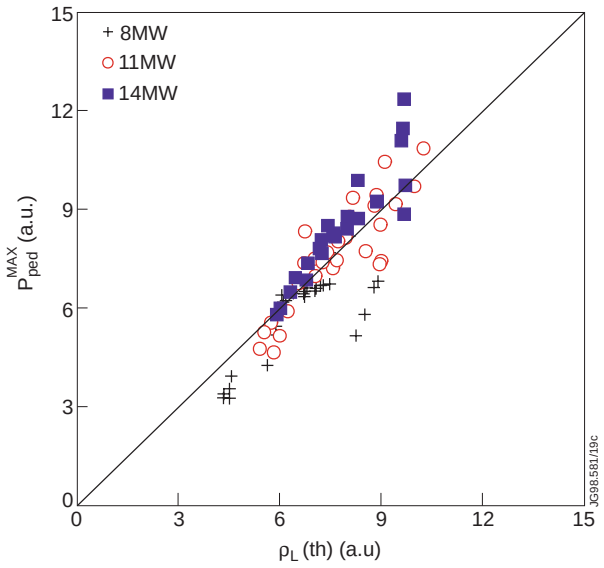

Figure 21: Maximum edge pedestal pressure plotted as function of the Larmor radius for thermal ions (normalised to the average of all data).

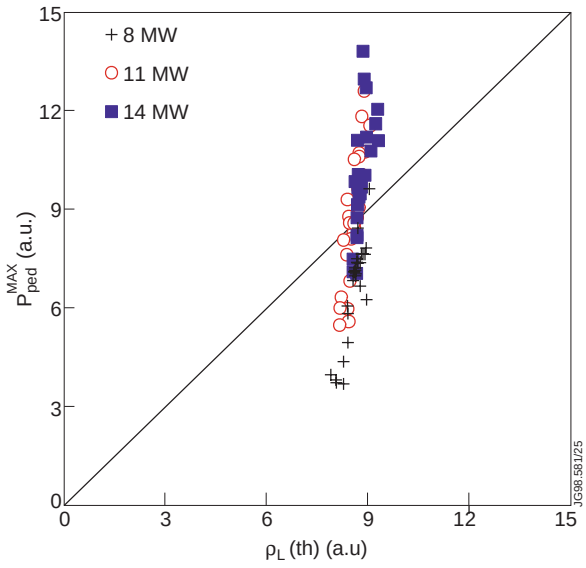

Figure 22: Maximum edge pedestal pressure plotted as function of the Larmor radius for fast ions (normalised to the average of all data)

As an example, for the series of discharges at 14MW, the drop of the $p_{ped,MAX}$ with fuelling in Type I ELMs is in excess of 50% of the unfuelled reference case. The corresponding variation of the fast ion average energy is too small to account for this pressure drop, since it goes from ~41keV to ~36keV, corresponding to a variation of the pedestal width of <10%. One reason for the difference between the results of this paper and those reported in [43] and [44] may be the different datasets used for the analysis. Whilst the dataset analysed in this paper includes gas fuelled, high density ELMy H-modes, the results presented in [43] and [44] contains unfuelled discharges only.

Figure 23 shows the variation of the fast ion density in the pedestal region as function of their energy, for the same discharges as in figures 21 and 22. The fast ion concentration n_i(fast)/n_e decreases as the density increases at the pedestal. As argued in [41], a critical density of fast ions is required for the suppression of the edge turbulence. One may speculate that the increase in the pedestal density drives the fast ion concentration below a critical value, although the decrease of n_i(fast)/n_e is due more to the density increase than to a reduction of the absolute number of fast ions in the pedestal region. The uncertainty in the theoretical determination of the critical number or fraction of fast ions required for the suppression of the turbulence, as well as the difficulties in the calculation of the fast ion density near the plasma edge [46], make it difficult to make a definitive statement.

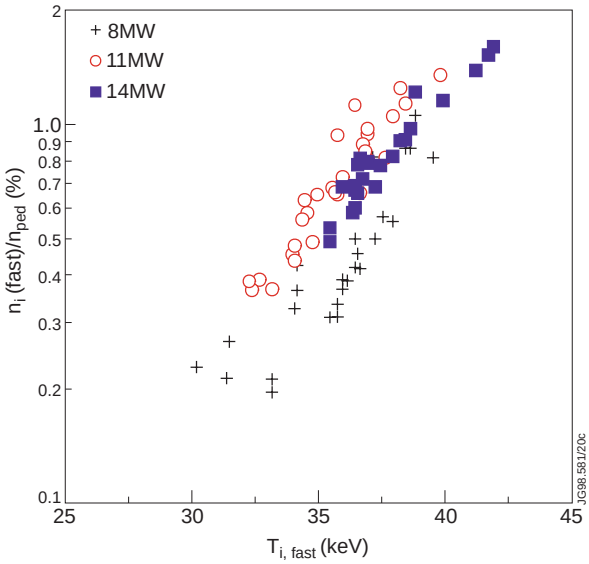

Figure 23: Fast ion fraction as a function of the fast ion average energy, for the power scan experiment described in the text. The fast ion fraction is calculated using the fast ion density profiles from the PENCIL code, divided by the pedestal electron density (n_e~n_i).

5.2.2 Isotope mass effects

The second set of experiments analysed is gas fuelled ELMy H-modes in pure H, D and T, at fixed plasma shape and input power (10-12MW P_{in}). Figure 24 shows the variation of the pedestal n_e and T_e for increasing gas fuelling, for the three isotopes and two plasma currents. The continuous lines in figure 24 are constant pressure curves, calculated as the average of $p_{ped,MAX}$ (Type I ELMs), for each series of discharges. The comparison of the experimental data with the curves shows that the edge pressure is not constant for increasing plasma density. The points that depart sharply from the constant pressure curve (particularly clear for the D and T at 2.6MA/2.7T) are data during steady state Type III ELMs.

These data have been analysed in a similar way to the power scan experiments described in 5.2.1, exploiting the variation of the mass of the plasma and of the plasma current. The data are plotted in a n_e-T_e diagram, to highlight the plasma current dependence of p_{ped}.

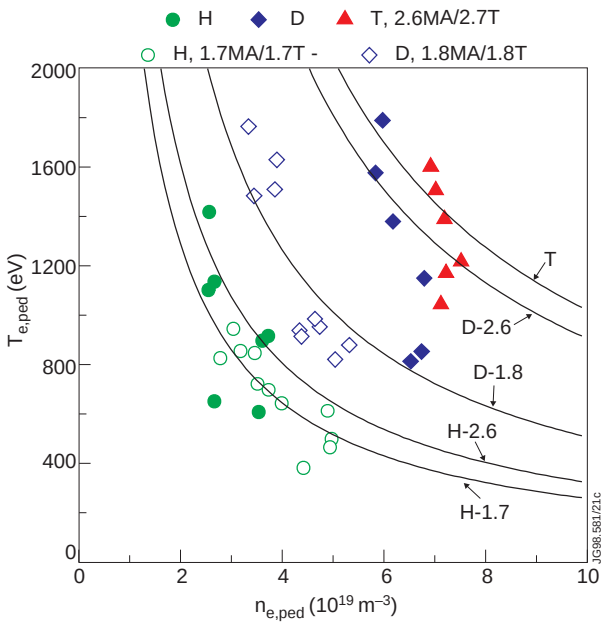

Figure 24: Evolution of the maximum edge pedestal n_e-T_e for 5 series of gas scans, at fixed plasma shape. Full symbols: 2.6MA/2.7T in H, D and T; open symbols: 1.7MA/1.7T in H and 1.8MA/1.8T in D. The n_e and T_e data are from LIDAR profiles at the fixed position of 3.75m.

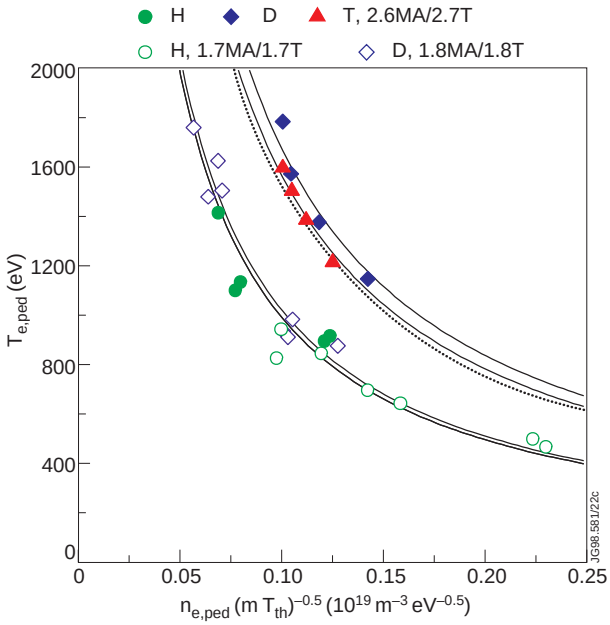

Figure 25: Edge pedestal temperature as function of the edge pedestal density normalised to $\sqrt{mT_{ped,th}}$, for the same set of data of the previous figure (see legend), excluding the high density Type III ELM points. The curves in the plot are calculated as described in the text.

Figure 25 shows the edge pedestal temperature plotted against the edge pedestal density divided by $\sqrt{mT_{ped,th}}$. If equation 2 describes our set of data and $\Delta \propto \rho_{L,th}$, we expect the data to be fitted by a hyperbole, and that the pedestal parameters from pulses at the same plasma current be described by a common curve. Moreover, the comparison of the data at 2.7 and 1.7-1.8MA should allow us to verify the expected plasma current dependence of $p_{ped,MAX}$ ($p_{crit} \propto I_p$). Referring again to figure 25, we see that this model describes very well the D and T data at 2.6MA/2.7T as well as the H and D data at lower current. The expected plasma current dependence is also confirmed by the data, as is shown by the dotted curve in the figure that is obtained by scaling the average best fit to the low current H and D data by the plasma current ratio 2.6/1.75.

Figure 25 also confirms that the edge pedestal pressure of the H discharges at 2.6MA/2.7T is not described by this simple model, since it should be the same as the D and T at the same current, and instead it follows a very similar trend to the low current pulses. Moreover, the model does not give a good fit to the

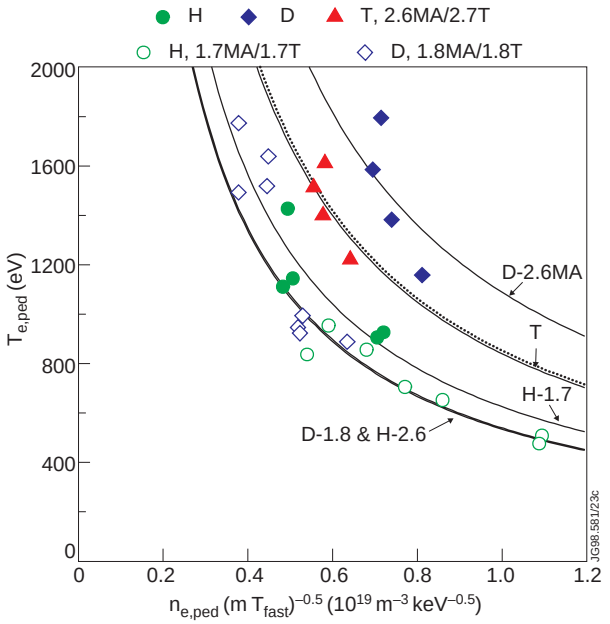

Figure 26: Edge pedestal temperature plotted against the edge pedestal density normalised to $\sqrt{mT_{fast}}$; same set of data as the previous figure.

data during the high density Type III ELMs (not shown): during the Type III ELMs the decrease of the edge pressure is faster with density than predicted.

For comparison, figure 26 shows the same set of data as figure 25, but this time the edge density has been normalised to $\sqrt{m}T_{fast}$. In common with the presently proposed model ($\Delta \propto \sqrt{m}T_{ped,th}$), this model does not describe either the high current H data (''transition'' type III ELMs) or the high density type III ELMs (the predicted edge pressure decay with density is even slower that in the previous model). However, although the fit for each single gas scan is acceptable, the fast ions Larmor radius model does not reproduce correctly the expected I_p dependence of $p_{ped,MAX}$ for the deuterium data at 2.6MA (the dotted line in the figure 26 is calculated by scaling the average of the best fit to the H-1.7MA and D-1.8MA data by 2.6/1.75, and is consistent with the T data at 2.6MA).

Edge magnetic shear scaling

Theoretical calculations of the stability of the plasma edge to ideal ballooning modes have been carried out for the case of elongated plasmas [47], and it is found that $(\nabla p)_{crit} \propto Sh^x$, with x>1.

In the experiment, at fixed I_p, B_t, isotopic mass and divertor geometry, the average plasma triangularity δ was varied from 0.14 to 0.38, corresponding to a variation of the edge magnetic shear from ~2.9 to ~4.1 (average values over the steady state phase of the discharges). Assuming that the pedestal width scales with $\rho_{L,th}$, we find that the peak pressure increases with the square of the edge magnetic shear (figure 27). This result is consistent with theoretical predictions, and with the analysis of experimental data presented in 43.

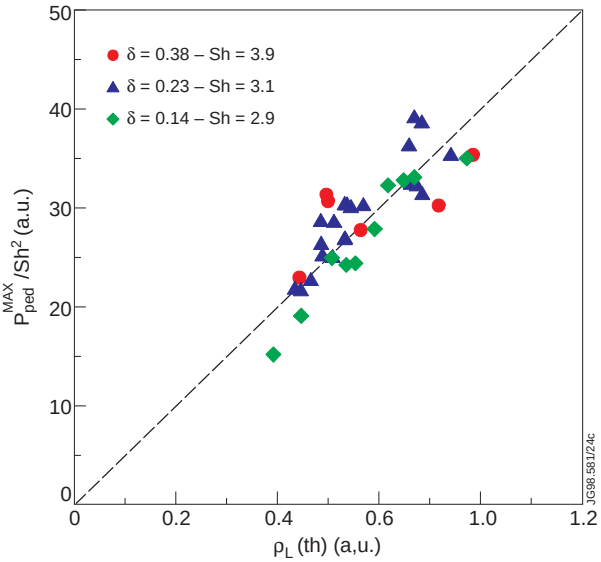

Figure 27: Peak edge pedestal pressure $p_{ped,MAX}$, normalised to the edge magnetic shear Sh^2, vs. the scaled pedestal width Δ, for a triangularity scan experiment at fixed I_p, B_t and isotopic mass of the plasma.

In summary, we find that the peak edge pedestal pressure in ELMy H-modes increases with input power, plasma current, edge shear and isotopic mass of the plasma. The simple model given in equation 2 adequately describes the variation of the pedestal pressure in these discharges with the above-mentioned parameters and with density/gas fuelling for type I ELMy discharges. The functional dependence for the shear and an expression for the pedestal width have been derived experimentally, and equation 2 now reads:

$$p_{ped,MAX} \propto I_p \, Sh^2 \sqrt{m}T_{ped,th} \qquad (3)$$

5.3 Comparison with JETTO/EDGE2 modelling

The JETTO transport code is based on a mixed Bohm/gyro-Bohm model for the plasma transport [48]. This model assumes that the transport inside the edge barrier is a combination of non-local Bohm transport and Gyro-Bohm local transport. In the model, the Bohm part dominates in the outer region of the plasma, whilst the central transport is gyro-Bohm dominated. The non-locality of the Bohm term is included via a coefficient of the form $(L_{Te,B})^{-1} \propto a\nabla T_e/T_e$, a= plasma minor radius).

This model, combined with the edge code EDGE2D/NIMBUS [19], was applied to the study of ELMy H-modes in JET [49]. The transport between ELMs is modelled with mixed Bohm/gyro-Bohm coefficients, and the transport in the barrier region is assumed to be neo-classical. The ELMs are triggered when the ideal ballooning limit is reached anywhere in the pedestal region. The ELMs are simulated by imposing an increase in the local edge transport ($\chi \geq 30 m^2 s^{-1}$) for 1ms. The transport barrier width was assumed to scale inversely to the edge pedestal temperature.

The results of this modelling are in qualitative agreement with the experimental results presented in this paper. In particular, the variation of the pedestal barrier width, which determines the pedestal top temperature and density, affects the global confinement of the plasma, consistently with the non-locality of the Bohm part of the energy transport coefficient. In the picture given by this model, the reduction of the pedestal temperature (due to increased neutral fluxes, for instance) is associated to an increase in the transport, that in turn causes further decrease of the temperature and the extension of the enhanced transport region.

The decrease of the pedestal width calculated by the code (due to the reduced local temperature) is associated to the ELM frequency increase.

This picture is consistent with the observed increase of the ELM frequency at high densities and also with the variation of the pedestal and profile components of the thermal stored energy with triangularity or density (section 5.1).

5.4 Isotopic effects in the SOL

In this section we discuss some preliminary results of simulations of the particle dynamics of H-modes in H, D and T carried out with the EDGE2D code, that provide interesting indications for the interpretation of mass effects.

H-mode plasmas in the three isotopes were simulated by EDGE2D, assuming a power flux to the SOL of $4.5 MWs^{-1}$ and by imposing neoclassical transport in the outer 5cm of the plasma, to simulate the edge transport barrier. The simulations were then carried out imposing a plasma density ramp and including an external gas source. One interesting result of the simulations is the decrease of the neutral flux across the separatrix with the isotope mass. In the code, at fixed plasma particle content, we find that the net neutral flux to the plasma core varies approximately as the ion thermal velocity ratio of the isotopes ($(\Phi_{ion})^H:(\Phi_{ion})^T \sim 1.7$), as one would

expect from basic atomic physics In the experiment, we see that similar plasma density is indeed achieved in H and D, for similar plasma parameters, but that the ELM frequency is much higher for the lighter isotope. The simulations also show that, for a given edge ion density, the temperature goes up with the mass of the isotope, in agreement with the trends of the experimental data.

This can be interpreted qualitatively in terms of difference in the local power balance. At constant input power, the increase of the neutral influx across the separatrix is associated to an increase of the charge exchange losses, causing a reduction of the local temperature and pedestal width Δ. In the code simulations, the charge exchange losses from inside the separatrix in H are approximately 40% higher than in T. If we assume that the critical pressure gradient at which an ELM is triggered is mass independent, the reduction in Δ would cause the ELM frequency to increase for decreasing isotope mass. In this sense, the reduction of the isotopic mass has the same effect on the edge parameters as increasing the gas puff rate. The results of these simulations imply that the effect of the mass on the edge pedestal stability is twofold: the edge pedestal width decreases at lower isotope mass due to the $\sqrt{m}$ dependence of the Larmor radius, but also due to the reduction of the temperature caused by increased charge-exchange losses. The enhanced neutral flux across the separatrix could also be invoked to justify the mass dependence of the H-mode threshold.

Work is in progress to improve the simulation to include explicitly ELMs, and to further analyse the experimental data, in order to verify the indications emerged so far.

6. SUMMARY

The study of ELMy H-modes presented in this paper has benefited from the unique capabilities of the JET tokamak. In fact, we have been able to carry out experiments varying independently the plasma current, the input power, the plasma shape, and also to study the isotopic effects including tritium. This flexibility has allowed us to investigate the characteristics of ELMy H-modes in detail, and to gain some understanding on the physics that governs the confinement of these type of discharges at high density.

Special technical preparation proceeded the experiments described. For the H-D-T comparison, high purity plasmas were obtained by carrying out full isotope change over of the walls and of the neutral beam systems for each isotope. The studies of the effects of the plasma triangularity were done making sure to maintain the same divertor geometry in all cases.

The maximum density achieved in steady state with gas fuelling in JET is ~95% of the Greenwald density limit. In general, the increase of the plasma density is associated to a decrease of the plasma thermal stored energy. Near the *GDL*, we observe a severe loss of both energy and particle confinement. This indicates that the H-mode density is limited by transport phenomena.

The analysis of the global energy confinement data confirms the result that the reduction of the confinement of high density plasmas (compared to the expected scaling) is a general

phenomenon, broadly independent of the specific parameters of the discharge, such as the input power, plasma shape, divertor geometry, isotope, etc. This is in contrast with the ITER97-P(y) scaling, that predicts better confinement at high density, as the stored energy is expected to scale as $n^{0.4}$. The effects of the plasma triangularity are particularly important; we find that the highest density and stored energy are obtained at the same time in steady state for plasma with high edge triangularity.

This result has prompted us to produce a new global energy confinement scaling to describe the high density ELMy H-modes (restricted for the time being to a subset of JET data). We find that a better fit to the data is provided by a scaling where the predicted thermal stored energy is independent of density and has a positive dependence on the plasma edge triangularity. The extension of the analysis to a larger database, including data from other tokamaks is required to produce an expression that can be used with confidence to extrapolate to a reactor.

The increase of the plasma density also causes changes in the plasma edge, most notably in the ELM frequency and type. At medium density, ELMy H-modes are characterised by Type I ELMs, that become more and more frequent as the density is increased, until we observe a transition to Type III ELMs. A decrease of the pressure at the top of the edge pedestal is observed as the ELM frequency increases. We have compared the pedestal energy content W_{ped} with the total plasma energy content W_{th}, as a function of the plasma density. At low and medium densities, the loss of thermal energy of the plasma is due to the decrease of the pedestal energy. At higher densities, the degradation of confinement extends within the edge transport barrier. Finally, in the Type III ELM regime at the highest densities, the whole pressure profile is lower than in equivalent unfuelled cases.

The last part of the paper studies the variation of the pedestal parameters with the input power, the plasma current, the edge triangularity and the isotopic mass of the plasma. In the analysis, we assume that the maximum edge pressure gradient in the pedestal region is limited by an ideal ballooning instability, and that we can approximate the edge pressure gradient as p_{crit}/Δ. We find that this simple model describes well the variation of the pedestal pressure, with the pedestal width scaling as $\sqrt{m}T_{ped,th}$. This result indicates that the Larmor radius of the thermal ions is related to the critical scale-length for the suppression of the turbulence in the edge pedestal region. A model, proposed by [41], where the stabilisation mechanism for the pedestal is provided by the fast ions, provides a good explanation for the differences in ELM type observed in ICRH and NB heated H-modes ([43] and [44]). However, the reduction in the pedestal pressure with increasing density is not well reproduced by the fast ion model. The dependence $p_{ped} \propto I_p\, Sh^2$ is common to the two models. The quadratic dependence of p_{ped} on the magnetic shear is obtained with a fit to the experimental data. Neither model describes the edge pedestal parameters of ELMy H-modes that are not in the Type I ELM regime. In particular, the low edge pressure of H-modes at low power (Type III ELMs of the transition) and of the high density Type III ELMy H-modes are not well represented by either scaling.

We have shown that changes in the pedestal parameters may influence the core energy of the plasma. This effect is experimentally observed, provided that the pedestal temperature is sufficiently varied (section 5.1). This result supports the mixed Bohm-gyro-Bohm model, where the region of enhanced transport may extend into the plasma core depending on the variations of the temperature at the top of the transport barrier.

Finally, EDGE2D/NIMBUS simulations give some insight into the isotopic effect observed in ELMy H-modes. The calculations show that the neutral influx across the separatrix increases inversely with isotopic mass. Higher influxes increase charge exchange losses, therefore the simulations predict lower edge temperatures for the lighter isotope, as observed experimentally. This result is consistent with the observed reduction of the edge pedestal pressure and increase in ELM frequency changing the isotope from T→D→H, all other conditions being equal.

7. ACKNOWLEDGEMENTS

The authors thank all JET Staff for the help and support in organising and running the experiments that are the basis for this paper.

REFERENCES

[1] AYMAR, R., THE ITER JOINT CENTRAL TEAM, and THE HOME TEAMS, Fusion Energy **1** (1996) 1, IAEA-CN-64/O1-1.

[2] KAMADA, Y., YOSHINO, R., USHIGUSA, K., et al Fusion Energy 1996 **1** (1996) 247, IAEA-CN-64/A1-6.

[3] MAINGI, R., MAHAVI, M.A., PETRIE, T.W., et al., "Density limit studies in DIII-D", to be published in Jour Nucl. Materials, 1998.

[4] MERTENS, V., KAUFMANN, M., NEUHAUSER, J., et al., Nuclear Fusion **37** (1997) 1607.

[5] GRUBER, O., MERTENS, V., NEUHAUSER, J., et al., Plasma Phys. Controlled Fusion **39** (1997) B19.

[6] The JET TEAM (Presented by G C Vlases), Fusion Energy 1996 **1** (1996) 371, IAEA-CN-64/A4-1.

[7] SAIBENE, G., BALET, B., CLEMENT, S., et al, "Steady state H-modes at high plasma density in JET", in Controlled Fusion and Plasma Physics (Proc. 24th Eur. Conf. Berchtesgaden, 1997), volume 21A, p.49, Geneva, 1997, European Physical Society, Part I.

[8] HORTON, L.D., VLASES, G.C., ANDREW, P., et al, "Studies in JET divertors of varied geometry (I): Non seeded plasma operation", submitted for publication in Nuclear Fusion, 1998.

[9] HORTON, L. and The JET Team, Plasma Phys. Controlled Fusion **38** (1996) A269.

[10] GREENWALD, M., BELL, M., EJIMA, S., et al., Nuclear Fusion **28** (1988) 199.
[11] ZOHM, H., Plasma Phys. Controlled Fusion **38** (1996) 105.
[12] CONNOR, J.W., Plasma Phys. Control. Fusion **40** (1998) 191.
[13] ITER Confinement Database and Modelling Working Group (presented by J.G. Cordey), Plasma Phys. Controlled Fusion **39** (1997) B115.
[14] CLEMENT, S., CHANKIN, A.V., CIRIC, D., et al., "Power deposition in the JET divertor during ELMs", to be published in Jour. Nucl. Materials, 1998.
[15] CHANKIN, A.V. and SAIBENE, G., "Interpretation of the edge operational diagram through similarity parameters for edge transport mechanism", submitted to Plasma Phys. Control. Fusion and JET-P(98)-22, 1998.
[16] SAIBENE, G., CHANKIN, A.V., CLEMENT, S., et al., "High density ELMy H-modes studies at JET in ITER relevant scenarios", to be published in the Proc. of the XXV Conf. on Controlled Fusion and Plasma Physics, paper {B-26}, Prague 1998, 1998.
[17] MERTENS, V., KAUFMANN, M., LANG, P., et al., "Edge density characterisation close to the Greenwald density limit with the new closed divertor in ASDEX upgrade", to be published in the Proc. of the XXV Conf on Controlled Fusion and Plasma Physics, Prague 1998, 1998.
[18] MATTHEWS, G.F., ZASTROW, K-D., ANDREW, P., et al., "Trace tritium and the H mode density limit", to be published in Jour. of Nucl Materials, 1998.
[19] TARONI, A., CORRIGAN, G., RADFORD, G., et al., Contributions to Plasma Physics **32** (1992) 438.
[20] The JET Team (presented by M. Keilhacker), Plasma Physics and Controlled Fusion **39** (1997) B1.
[21] RIGHI, E., BARLETT, D.V., CHRISTIANSEN, J.P., et al., "Isotope scaling of the H-mode power threshold in tritium, deuterium-tritium, deuterium and hydrogen plasmas on JET", submitted for publication in Nuclear Fusion, 1998.
[22] BRAITHWAITE, G., GOTTARDI, N., MAGYAR, G., et al., Rev. Sci. Instr. **60** (1989) 2825.
[23] BARTLETT, D.V. et al., "Recent progress in the measurements and analysis of ECE in JET", Proceedings of the 9th Int. Workshop on ECE and ECRH}, Borrego Spring (USA), volume EC-9, p. 511, 1995.
[24] GOWERS, C., BROWN, B., FAJEMIROKUN, H., et al., Rev. Sci. Instrum. **66**(1) (1995) 471.
[25] HAWKES, N.C. and PEACOCK, N.J., Rev. Sci. Instr. **63**(II) (1992) 5164.
[26] COX, M., "FOKMEG: A package to determine the fast ion distribution function for the JET interpretation code suite", Technical Report KR5-33-04, UKAEA Culham Laboratory, UK, 1988 Report on a JET contract.
[27] GOLDSTON, R.J. et al., J. Comput. Phys. **43** (1981) 61.

[28] CAMPBELL, D., CLEMENT, S., GOTTARDI, N., et al., “The density limit in JET diverted plasmas”, in Controlled Fusion and Plasma Physics (Proceedings of the 21st European Conference, Montpellier)}, volume 18C, Part I, p.2, 1994.

[29] KASS, T., GUNTER, S., MARASCHEK, M., et al., Nuclear Fusion **38/1** (1998) 111.

[30] MARASCHEK, M., GUNTER, S., KASS, T., et al., MHD characteristics of ELMs and their precursors, to be published in the Proc. of the XXV Conf. Controlled Fusion and Plasma Physics , Prague 1998, 1998.

[31] HUIJSMAN, G., “External Resistive Modes in Tokamaks”, PhD thesis, Free University of Amsterdam (Holland), 1991.

[32] RIGHI, E., BARTLETT, D., CONWAY, G.D., et al., “The role of edge parameters in the H-mode transition in JET”, in Controlled Fusion and Plasma Physics (Proc. 24th Eur. Conf. Berchtesgaden, 1997), volume 21A, p.93, Geneva, 1997, European Physical Society, Part I.

[33] The JET Team, (presented by R D Monk), “Recent results from divertor and SOL studies at JET”, to be published in Fusion Energy 1998 {IAEA-CN-69/EX6/4}, 1998.

[34] The JET TEAM (Presented by D. Stork), Fusion Energy 1996 **1** (1996) 189,IAEA-CN-64/A1-1.

[35] KUPSHUS, P., DE HAAS, J.C.M., GADEBERG, M., et al., “Experiments on plasma fuelling and ELM control by pellet injection on JET”, in Controlled Fusion and Plasma Physics (Proc. 24th Eur. Conf. Berchtesgaden, 1997)}, volume 21A, p.45, 1997, Part I.

[36] ASAKURA, N., SHIMIZU, K., SHIRAI, H., et al., Plasma Phys. Control. Fusion **39** (1997) 1295.

[37] The JET TEAM, (Presented by K Thomsen), “H mode power threshold and confinement in JET H, D, D-T and T plasmas”, to be published in Plasma Phys. Control. Fusion, 1998.

[38] HORTON, L.D., SARTORI, R., BALET, B., et al., “High fusion power steady-state operation in JET D-T plasmas”, submitted for publication to Nuclear Fusion, 1998.

[39] FISHPOOL, G.M., Nuclear Fusion **9** (1998) 1373.

[40] ZHANG, W., TUBBING, B.J.D., and WARD, D.J., Plasma Phys. Control. Fusion **40** (1998) 335.

[41] PARAIL, V., GUO, H.Y., and LINGERTAT, J., “Fast particle and the edge transport barrier”, to be published in Nuclear. Fusion, 1998.

[42] NAVE, M.F.F., LOMAS, P.J., ALPER, B., et al., “Discharge optimisation and the control of MHD modes”, to be submitted for publication to Nuclear. Fusion, 1998.

[43] LINGERTAT, J., BHATNAGAR, V., CONWAY, G., et al., “The edge operational space in JET”, to be published in Jour. Nucl. Materials, 1998.

[44] BHATNAGAR, V., LINGERTAT, J., BARNSLEY, R., et al., “Edge localized modes and edge pedestal in NBI and ICRF heated H, D and T plasmas in JET”, submitted for publication in Nuclear Fusion, 1998.

[45] HATAE, T., KAMADA, Y., ISHIDA, S., et al., Plasma Phys. Control. Fusion **40** (1998) 1073.

[46] ZASTROW, K-D., ANDREW, P., BASSE, N.P., et al., “Particle transport in steady state ELMy H-modes studies by trace tritium injection during JET DTE-1”, to be published in the Proc. of the XXV Conf. on Control Fusion and Plasma Phys, paper B-179, Prague 1998, 1998.

[47] POGUTSE, O.P. and YURCHENKO, E.I., Rev. of Plasma Phys. **2** (1986) 65.

[48] The JET TEAM, (Presented by A Taroni), Fusion Energy 1996 **2** (1996) 477, IAEA-CN-64/D3-3.

[49] TARONI, A., CORRIGAN, G., LINGERTAT, J., et al., Contrib. Plasma Phys **1/2** (1998) 37.